REAR-DETECTION PHOTOTHERMAL TECHNIQUE FOR MICROSCALE THERMAL DIFFUSIVITY MEASUREMENT

by

Dihui Wang

B.S., Xi'an Jiaotong University, 2016

Submitted to the Graduate Faculty of

Swanson School of Engineering in partial fulfillment

of the requirements for the degree of

Master of Science

University of Pittsburgh

2019

UNIVERSITY OF PITTSBURGH

SWANSON SCHOOL OF ENGINEERING

This thesis was presented

by

Dihui Wang

It was defended on

March 29, 2019

and approved by

Heng Ban, Ph.D., Professor
Department of Mechanical Engineering and Materials and Science

Qingming Wang, Ph.D., Professor
Department of Mechanical Engineering and Materials and Science

Sangyeop Lee, Ph.D., Assistant Professor
Department of Mechanical Engineering and Materials and Science

Thesis Advisor: Heng Ban, Ph.D., Professor
Department of Mechanical Engineering and Materials and Science

REAR-DETECTION PHOTOTHERMAL TECHNIQUE FOR MICROSCALE THERMAL DIFFUSIVITY MEASUREMENT

Dihui Wang, M.S.

University of Pittsburgh, 2019

In nuclear reactors, a characteristic of irradiated nuclear fuel is that its microstructure is damaged by neutron irradiation, thus, the local changes of thermal diffusivity are existed. Additionally, extremely large temperature gradient ($\sim 1600 \mathrm{K/cm}$) from the fuel centerline to the coolant result in similar gradient of thermal diffusivity. However, most existing thermal diffusivity measurement techniques do not have the high spatial resolution ability. Therefore, for better understanding the spatial distribution of nuclear fuel thermal diffusivity and minimizing the radiation exposure of experiment sample, the objective of this study is to develop a non-contact thermal diffusivity measurement technique with high spatial resolution for sample of micrometer-sized.

Based on photothermal reflectance technique (PRT), this study developed a new approach that the thermoreflectance signal is measured at the rear surface of the Focus ion beam (FIB) fabricated micrometer-sized sample. An analytical model was built for this Rear-Detection Photothermal Reflectance Technique (RDPRT) to guide the experiment and optimize the FIB sample design. Metal with High absorptivity at heating laser wavelength was coated on the front surface of sample to ensure good energy absorption.

Metal with high thermoreflectance coefficient at probe laser wavelength was coated on the rear surface of sample to ensure high signal to noise ratio of the measurement. An experimental measurement system was designed and built for the FIB sample. The experiment result shows good agreement to the literature value, with uncertainty under 6%. Sources of experimental uncertainty are analyzed qualitatively and quantitatively. The RDPRT enables thermal property measurement at a high spatial resolution for FIB sample and offers unique option for measurements of special materials, such as irradiated nuclear fuel or other irradiated materials to minimize radiation exposure.

TABLE OF CONTENTS

LIST OF TABLES

Page

LIST OF FIGURES

Page

PREFACE

ACKOWLEDGMENTS

First, I would like to express my sincere gratitude to my advisor, Dr. Heng Ban, for his incessant enthusiasm and inspiration throughout these two years. I still remember our first meeting, from which I have determined what kind of person I want to be. Dr. Ban gives me advices not only about how to do research, but also about how to lead a successful life.

Also, I would like to thank all my lab mates and staff at University of Pittsburgh, for all their valuable discussion and selfless help. Special thanks go to Zhuorui Song, who gives me most assistance on my project work. The same thanks should be sent to Lin Zhang and Binxing Zhao, Zeke Villareal, Tate Shorthill, Yuan Gao, they are my workmates as well as my greatest friends. I also owe my gratitude to many friends who encourage me to finish this course. Ruikai Liu, Zhijie Zhang, Caojian Chang and Lifu Huang always supported me whenever I needed them; Brady Cameron, Chukun Xia and Xinlu Zhang inspired me to find interest in other area of life. Limitation of space prevents from listing all the names here, but I cherish your friendships by my heart and soul.

My deepest appreciation goes to all my family members. I cannot be more grateful for the help, encouragement, support and love they give me in every moment of my life.

Dihui Wang

NOMENCLATURE

D	Thermal diffusivity, [m^2/s]
D_f	Thermal diffusivity of film, [m^2/s]
D_s	Thermal diffusivity of substrate, [m^2/s]
L	Length, [m]
L_{th}	Thermal diffusion Length, [m]
Q	Heat flux, [W/m^2]
T	Temperature, [K]
T_f	Temperature of film, [K]
T_s	Temperature of substrate, [K]
c	Specific heat capacity[$J \cdot kg^{-1} \cdot K^{-1}$]
c_f	Specific heat capacity[$J \cdot kg^{-1} \cdot K^{-1}$]
c_s	Specific heat capacity[$J \cdot kg^{-1} \cdot K^{-1}$]
f	Frequency, [Hz]
h	Film thickness, [m]
k	Thermal conductivity,[$W \cdot m^{-1} \cdot K^{-1}$]
k_f	Thermal conductivity,[$W \cdot m^{-1} \cdot K^{-1}$]
k_s	Thermal conductivity,[$W \cdot m^{-1} \cdot K^{-1}$]

q Thermal wave number, [m^{-1}]

t Time, [s]

w Width, [m]

α Optical absorption coefficient, [m^{-1}]

α_f Optical absorption coefficient, [m^{-1}]

α_s Optical absorption coefficient, [m^{-1}]

β The ratio of the substrate thermal effusivity to the film thermal effusivity

δ Phase(lag), [deg]

$\delta(x)$ Dirac delta function

ω Angular frequency, [Hz]

1.0 INTRODUCTION

In this chapter, three essential thermal properties of heat conduction are discussed, including thermal conductivity, diffusivity, and effusivity. Two important concepts: Thermal wave and Thermal diffusion length are explained. The necessity of this project is stated in the end.

1.1 Definition of Heat Transfer

Heat transfer is thermal energy in transit due to a spatial temperature difference [1], there are three types of heat transfer modes: heat conduction, heat convection, and heat radiation. It has been established that heat conduction is the main mode of heat transfer in solid material, it occurs when a temperature gradient exists in a stationary medium, which could be a solid part or a fluid part. Heat convection occurs between a moving fluid and a surface. The third kind of heat transfer is heat radiation, which occurs between two non-contacting surfaces at different temperatures, without the need for an intervening medium [2]. The model of heat transfer of multi-layer materials used in this project is heat

conduction, thus it is necessary to discuss three thermal properties of heat conduction : thermal diffusivity and thermal conductivity and thermal effusivity.

1.1.1 Thermal conductivity

Thermal conductivity is the most basic thermal property in heat conduction. From definition in current textbook [3], heat transfer process can be quantified in terms of appropriate rate equation. In terms of heat conduction, the rate equation is known as *Fourier's Law*, which explains the relation between heat flux and temperature gradient in homogeneous solid material. For one-dimensional (1D) application, the rate equation can be written as:

$$q''_x = -k\frac{dT}{dx} \tag{1.1}$$

where heat flux $q''_x(W/m^2)$ is the heat transfer rate in x-direction per unit area. the minus sign on RHS represents the fact that the heat flux's direction is from high temperature to low temperature. The parameter k $(\mathrm{W/m \cdot K})$ is thermal conductivity, which represent the ability of material to transfer heat and is a characteristic of the material. In some literatures, thermal conductivity is also known as λ. $\frac{dT}{dx}$ is the temperature gradient.

Thermal conductivity can vary greatly depends on type of materials. Metals like copper, aluminum and silver have thermal conductivity above 100 (W/ (m · K)). The main energy carrier for heat conduction in metals is electrons. In contrast, most non-metallic material such as balsa wood, carbon, earth have thermal conductivity around 1 $(\mathrm{W/(m \cdot}$

K)). To elucidate the facts, it is necessary to introduce vibration motion in microstructure. In 1912, Debye stated that the fundamental heat transfer mechanism in non-metal crystalline material is the wave motion by lattice vibration. Fig1, adapted from "Review of thermal conductivity in composites" by N. Burger [4, 5], explains the mechanism of thermal energy transfer through vibration motion in crystalline structure.

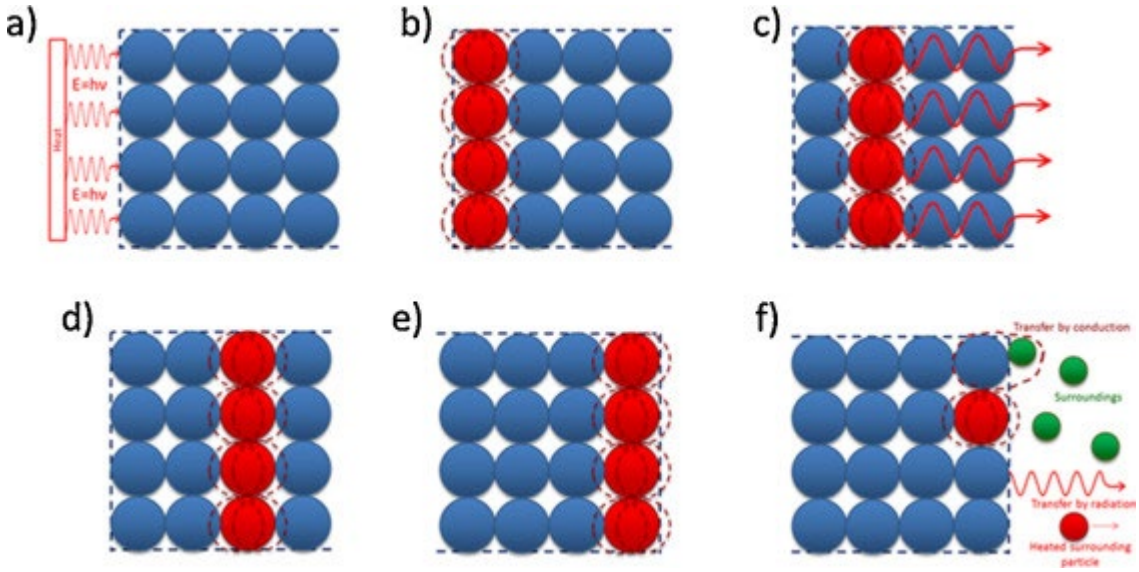

Figure 1-1 Thermal Conductivity mechanism in crystalline structure [5]

The representation in Fig.1 describe the vibration of initial atom leads to partial vibration to the next atom(s), conducting further into the material. For an isotropic three-dimensional material, thermal conductivity can also be analytical obtained by the Debye equation [6]:

$$k = \frac{C_p v l}{3} \tag{1.2}$$

where v is average phonon velocity, l is the phonon mean free path. Compare to metals, non- metallic materials have much lower number density of free electrons and longer phonon mean free path, which explains that most metals are better thermal conductor than non-metallic materials. There are other facts such as number density, crystalline structure and existence of defect, which can be calculated by the Bose-Einstein equation.

1.1.2 Thermal diffusivity

Thermal diffusivity is the thermal properties of interest in this work, which plays a very important role in transient heat transfer analysis. It can be derived from thermal conductivity divided by density and specific heat capacity at constant pressure [7] as shown in Eq. (1.3).

$$\mathrm{D} = \frac{k}{\rho c_p} \tag{1.3}$$

Together, ρc_p can be considered as a new parameter, the volumetric heat capacity (J/(m³·K)). In the same way, by acknowledging thermal diffusivity, thermal conductivity could be acquired by Eq. (1.3) as well. As seen in the transient heat transfer equation [4],

$$\frac{\partial T}{\partial t} = D\nabla^2 T \tag{1.4}$$

Thermal diffusivity is as the ratio of the time derivative of temperature to its curvature, a property of a material that describe the rate of heat transfer from hot side to cold side. In a sample with high thermal diffusivity, heats could move rapidly cross it since the material conducts heat quickly relative to c_p.

1.1.3 Thermal effusivity

Thermal effusivity may be the least familiar thermal parameters in these three parameters. In thermodynamics, thermal effusivity is defined as square root of the material's thermal conductivity and its volumetric heat capacity:

$$\mathrm{e} = (\mathrm{k}\rho c_p)^{1/2} \tag{1.5}$$

where volumetric heat capacity is defined as above, the product of ρ and c_p. Thermal effusivity is an indicator of material ability to exchange thermal energy with its surrounding. It determines the interface temperature of two different-temperature semi-infinite objects brought into contact:

$$T_m = T_1 + (T_2 - T_1)\frac{e_2}{(e_2+e_1)} \tag{1.6}$$

where T_m is the temperature of contact surface; $T_1, e_1 and \quad T_2$, e_2 are temperature, thermal effusivity of two separate semi-infinite bodies. It is also a good first guess for two finite bodies.

1.1.4 Thermal diffusion length

Thermal diffusion length is another parameter used in this paper, which is very important in frequency domain photothermal technique and periodic heating. It is defined as the square root of the thermal diffusivity of the material over the frequency of the heat wave/ periodic heating on the sample surface [4]:

$$L_{th} = \sqrt{\frac{D}{\pi f}} \tag{1.7}$$

Thermal diffusion length is always used in cases when a sinusoidal heat source is applied to a sample and where thermal wave is produced. In contrast to other types of waves such as elastic, attenuation of thermal wave is extremely fast. In order to quantify the distance of the heat-wave propagation, thermal diffusion length has been introduced, it represents the distance at which the amplitude decreases to *1/e* compare to surface. By varying frequency, it is possible to control heat propagation depth, which will also affect the sensitivity of different thermal properties in different layer [6]. It is the fundamental reason that frequency-domain PRT can be applied in multi-layer samples.

1.1.5 Other used concepts

Thermoreflectance coefficient, which is an important thermal parameter for choosing coating materials. It describes the optical reflectivity change due to temperature change, higher thermoreflectance coefficient in probe laser wavelength range could leads to higher sensitivity to temperature change on sample's surface and increase the signal to noise ratio of the measurement [9].

Thermal Wave, which is introduced by Carslaw and Jaeger in the classic work [2] Conduction of Heat in Solids. In the book, the temperature expression is derived from periodic heat source thermal conduction equation was proved to be a wave-like function, changing periodically in both space and time. This "thermal wave" also showed other wave

propagation feature such as reflection, refraction and transmission. Since then, the concept thermal wave has been widely used to describe temperature oscillations produced by a periodic heat source

1.2 Motivation

Thermal diffusivity is one of the most important thermal property related to rate of heat transfer and reactor safety. A characteristic of radiated nuclear fuel is that its microstructure is damaged by neutron irradiation, thus, unequal and local changes of thermal diffusivity could be significant. However, most of current in-pile thermal diffusivity measurement techniques for nuclear fuel cannot quite satisfy the high spatial resolution requirement. For example, thermocouples are applied to measure the temperature gradient in the nuclear fuel, which could only provide an "effective" thermal diffusivity of the fuel, cladding and gap [11]; The laser flash technique, another commonly deployed measurement technique, also does not have high spatial resolution [12].

Therefore, a more suitable measurement technique is needed. The main motivation of this project is to develop a measurement technique of solid materials (ultimately, nuclear fuels) with micrometer-resolution, and only requires a small surface area for measurement, which would also contribute to minimal sample radiation level of nuclear materials and get the spatial distribution of thermal property.

1.3 Thesis Overview

This thesis is consisted of three main parts. In Chapter 2-4, A literature review, objectives and theoretical model are given respectively, several current photothermal techniques are discussed in Chapter 2; A 1D model for rear-detection PRT using thermal wave method is explained and sensitivity analysis is made in Chapter 4. In Chapter 5 and 6 the experimental details are given, including experimental setup, sample preparation, result and uncertainty analysis. In the end, Chapter 7 gives the conclusions and future plans.

2.0 LITERATURE REVIEW

In this chapter, traditional measurements of thermal properties and photothermal techniques are reviewed. Including traditional analytical solution and several photothermal techniques, advantages and shortcomings are discussed.

2.1 Traditional Measurements of Thermal Properties

In 1753, Benjamin Franklin was the first one realizes that different materials have different abilities “to receive and convey away the heat”, then experimental study about thermal conductivity began in the eighteenth century. Thermal conductivity was later defined by the basic heat conduction equation by the French Scientist J.B.J Fourier in 1822:

$$\frac{Q}{A} = -k\frac{\partial T}{\partial x} \tag{2.1}$$

Eq. (2.1) is also the fundamental equation for one of two tradition measurement, steady-state measurement. For steady-state measurements, a constant source of heat is needed, which aim to acquire a steady temperature gradient $\frac{\partial T}{\partial x}$ on sample. From known heat flux and area, heat conductivity can be obtained. One problem of steady-state measurement is that it always requires a relative long period of time to reach steady state; another problem is the existence of contact resistance of thermometers is inevitable and it would influence the accuracy greatly especially when the sample’s thermal conductivity is

high. With these limitations, steady-state method is suitable for samples with low thermal conductivity, and applications with no local measurement requirement.

To eliminate those limitations of steady-state methods, non-steady-state methods, known as transient method, is developed. One type of transient methods uses periodic heat wave to heat sample and the time-dependent temperature responses is recorded, then using transient heat conduction equation to obtain thermal properties. Periodic heating method was developed by Ångström in 1861[11]. He uses a harmonic heating source to create the periodic temperature response, from obtained amplitude and phase lag of the temperature response, thermal properties are derived. To go further, pulsed heat source, such as pulsed laser [13], is second kind heating source of transient method. From the temperature response due to short excitation, thermal properties can be obtained. These two-classic types of transient method are basis of photothermal techniques in frequency domain and time domain respectively [14].

Although transient methods is absolutely more intricate than steady-state method to obtain, high spatial resolution is required in this study. Thus, transient photothermal method is used.

2.2 Photothermal Techniques

Photothermal (PT) techniques was founded by Rosenzwaig and Kreuzer [15] in 1970s. Photothermal techniques have developed into several branches, each of them using specific physical effect to do measurements, with the common feature that uses a light source to shine on sample to provide thermal excitation. Light energy absorbed would heat the sample, and this heat triggers temperature changes along with changes of the sample thermal properties which are related to temperature. The fundamental basis of photothermal techniques are the measurement of the temperature, pressure or density changes due to optical absorption [16].

There are several intrinsic advantages of photothermal techniques: PT techniques have very good local measurement ability, some have microscale or nanoscale spatial-resolution; PT techniques are non-contact methods and won't destruct the sample; the test can be done in a short time. Today a wide range of methods can be subsumed under this heading, several popular photothermal techniques will be presented in following sections.

2.2.1 Photoacoustic spectroscopy

The photoacoustic (PA) effect is the process of acoustic wave generation in a sample resulting from the absorption of light (photons). This phenomenon was first detected by Bell, Rontgen, and Tyndall in 1880. Sunlight was used as light source at first. Sunlight was

focused onto a sample within a cell which was connected to a listening tube. When the sunlight was repeatedly blocked and unblocked, the sunlight chopping frequency will be detected through the listening tube. Laser source has taken the place of sunlight as light source in 1968 and PA became widely used to measure thermal properties.

The basic theory of photoacoustic detection is based on the phenomenon that a fraction of the ground-state molecular in sample will be exited into higher energy level due to absorption of light. These excited molecules will then subsequently relax through a combination of radiative and non-radiative pathways. The non-radiative component will produce heat within the lighted region, along with sound wave generated by thermal expansion. The pressure wave could be detected with a suitable sensor such as a microphone used for a gaseous sample. To improve the detection sensitivity, Lock-in amplifier has been added in to the measurement system.

Rosencwaig and Gersho were pioneers who used PA technique to measure thermal diffusivity in 1975, Optical-thermal conversion efficiency was considered in heat diffusion equations, and they derived the AC component of the temperature distribution and the gas displacement under periodic laser-excitation as functions of the thermal diffusivities of the gas and sample. Similar method was applied to detect thermal conductivity [17,18]. The apparatus of photoacoustic spectroscopy is as shown below (Fig.2-1) [19]:

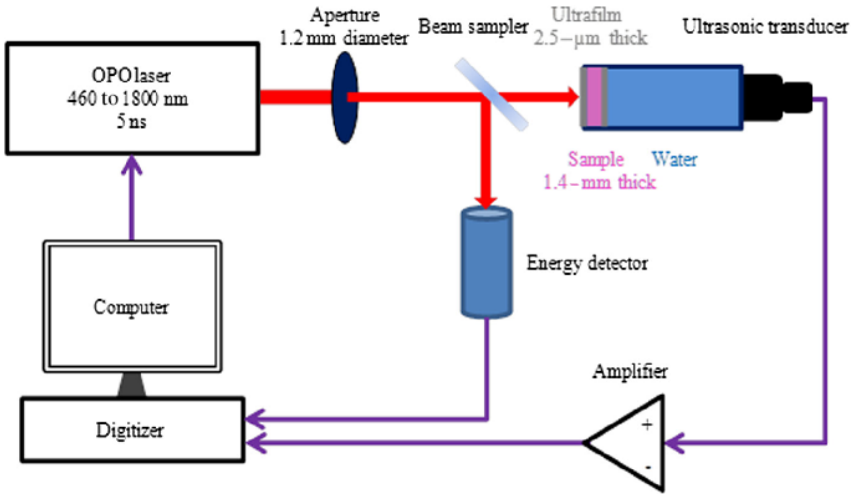

Figure 2-1 apparatus of photoacoustic spectroscopy [19]

2.2.2 Laser flash technique

Laser flash method is another widely used method to experimentally determine thermal diffusivity, which was first described by Parker et al.1961 [20]. The principle of laser flash measurement assumes that an infinite flat sample has a thickness L, was put inside a furnace which has a uniform initial temperature. Then an instantaneous, spatially uniform energy pulse was applied at sample's front surface, which would subsequently cause a temperature increasing in the rear surface, the temperature rise can be detect by an IR detector. Flash tube was firstly used as heat source due to technology limitation, and laser heating has become standard nowadays. The sample is ideally opaque, homogeneous and isotropic [21]. Thermal properties of sample are also ideally constant, with negligible change within the temperature rise interval (between 2-10 °C). When these two requirements are satisfied,

one-dimensional heat transfer model can be established in the x direction (along thickness) [22]. By the analysis of Parker et al, thermal diffusivity can be expressed as:

$$\alpha = 0.1398L^2/(t_{0.5}) \tag{2.2}$$

where$L$ is the thickness of sample, $t_{0.5}$ is the time length for the rear-surface temperature to reach half of its maximum value. Experiment conditions must closely represent those assumptions made in last paragraph to ensure accuracy. The laser flash system is as shown below:

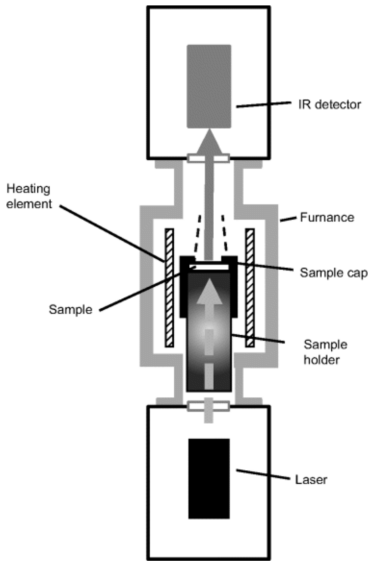

Figure 2-2 Laser flash method system [21]

Several potential limitations are existing for applying flash technique, most of these limitations due to the ideally assumption: opaque, homogeneous and isotropic samples as well as zero heat loss [23]. Although most of them are solved in the last 20 years [24-26], some of problems are still unsolved [21]:

1) Optimum half-rise time is 40-100 ms, which depends on sample's thickness and diffusivity values. Due to finite-pulse-time (τ) effects, which means that the laser heating process is not instantaneous and has a duration around 1ms, large $\tau/t_{0.5}$ ratio would cause result has large uncertainty.

2) Very thin sample may suffer from greater surface damage during sample preparation and cannot ensure requirement of homogenous. Thus, to guarantee accuracy, different materials have different thickness minimum requirement.

2.2.3 Photothermal radiometry

Photothermal radiometry (PTR) was first introduced by Nordal and Kanstad in 1979, which is based on detection of transient heat-flux emission of thermal radiation of the heated sample [27, 28]. Santos and Miranda developed PTR signal in frequency domain and time domain including optical absorption in 1981, which applied PTR technique to measure thermal diffusivity and the coefficient of optical absorption of solids [29]. Several groups have used PTR techniques to measure various material thermal properties [30-33].

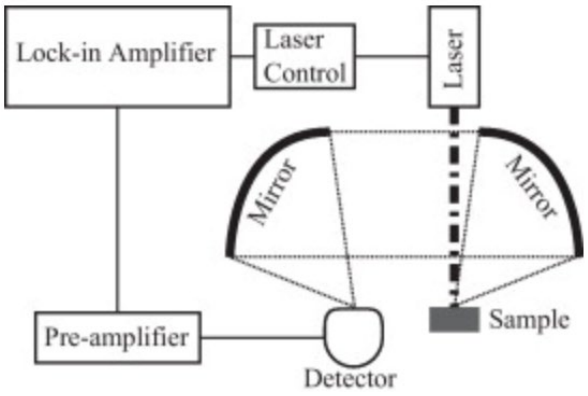

Figure 2-3 PTR setup [29]

2.2.4 Photothermal reflectance technique

The photothermal reflectance technique (PRT) is based on the approximation that the optical reflectivity of solid material is a linear function of the temperature change [34]. It was first developed by Rosencwaig in 1985 [35]. An intensity-modulated heating laser is applied to heat the sample, and another constant intensity probe laser is applied to measure to thermal wave propagation by optical reflectance, as an indicator of temperature change. Thus, in order to increase the sensitivity of measurement, high absorptivity at heating laser wavelength, high thermoreflectance coefficient as well as high reflectivity at probe laser wavelength are required for sample's material. These requirements can be achieved by coating certain type of metal film. To go further, three types of photothermal reflectance technique have been developed: frequency domain technique (FDPRT) [36-38], spatial domain technique (FDPRT) [39] and time domain (TDPRT) [40,41]. A typical PRT system setup is shown below:

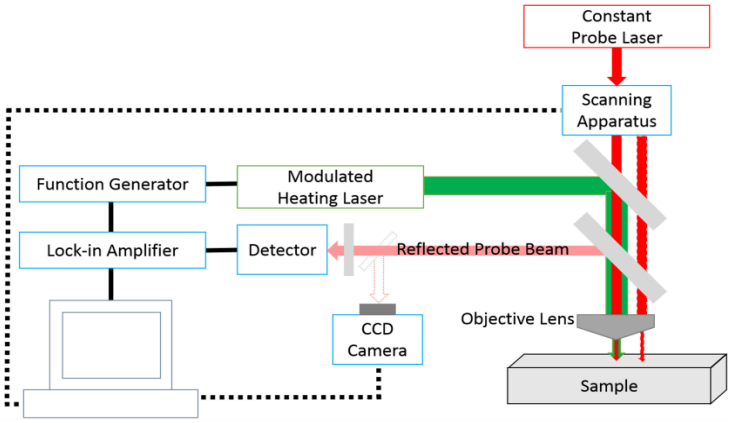

Figure 2-4 Typical PRT system setup [42]

PRT is suitable for system operates in open environment, employ completely non-contact and non-damage method for both heating and probing, and with microscale resolution. The diameter of heating laser and probe laser spot can be as small as one micron, which requires the distance between heating laser spot and probe laser spot be controlled at microscale precisely. It can be realized by applying a motorized stage to adjust the light path of either heating laser or probe laser. However, the employment of motorized stage and other complicated light path setup limits PRT to be used only in the research labs. No report shows that PRT has been used in industry or in situ application successfully [43].

Photothermal reflectance techniques have been applied to measure thermal properties with high spatial resolution successfully [43]. SDPRT was first developed by Fanton, which applied the theory of Angstorm, measuring phase lag on sample's surface caused by scanning probe laser on sample surface. Thermal diffusivity can be obtained from the phase lag-separation slope in a straight forward manner [44]. Recently, thermal diffusivity has

been measured by SDPRT successfully on focus ion beam (FIB) fabricated micrometer-sized sample [46].

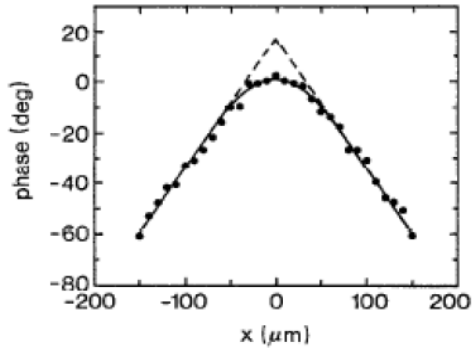

Figure 2-5 Phase lag-separation result of SDPRT[44].

Another photothermal technique is frequency domain photothermal reflectance technique (FDPRT), which is the most popular photothermal technique to measure thermal properties of film-substrate samples nowadays. Instead of moving stage, FDPRT applies fixed heating laser and probe laser light path and they are kept concentric while varying heating frequency and recording the phase-lag at each frequency.

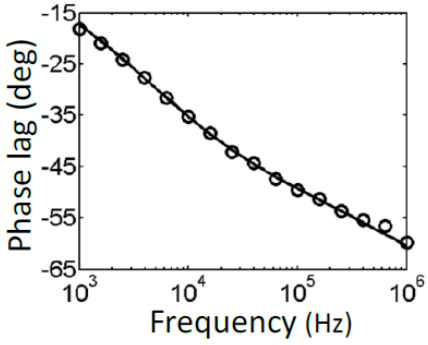

Figure 2-6 An example of FDPRT experiment data [45]

2.3 Conclusion of Literature Review

Based on comparison between different photothermal techniques, the photothermal reflectance technique is chosen in this application as it is the most promising thermal properties measurement method. Photoacoustic methods have stringent requirements on experiment setup, signal-to-noise ratio is also hard to warrant; the laser flash methods have large uncertainty in thin samples measurement and don't have local measurement ability; and photothermal radiometry have a resolution limitation.

Classic PRT applies heating laser and probe laser on same side of sample surface, Titanium and gold are popular coating material. However, it is hard for a single kind metal material to satisfy both high absorptivity at heating laser wavelength and high thermoreflectance coefficient at probe laser wavelength. It leads to dilemma whether sacrifice heat intensity sample can receive, or probe signal intensity. For spatial domain measurement, uncertainty would increase when the sample is anisotropic, and the experiment alignment is difficult.

To minimize radiation of nuclear fuel sample, focus ion beam (FIB) fabricated micrometer-sized sample needs to be applied, for example, $(11 \times 18 \times 2)\mu m^3$. However, the micrometer-scale thickness of designed sample does not satisfy the infinite-thickness requirement of classic FDPRT model.

Thus, an improved measurement method is needed. In this project, a rear-detection PRT is developed to solve these problems. Metal with high absorptivity at heating laser

wavelength is coated on front side to ensure good energy absorption, metal with high reflectivity and thermoreflectance coefficient at probe laser wavelength is coated on rear side to ensure high signal to noise ratio. For this rear-detection method, finite-thickness model is applied which is suitable to micrometer-sized sample.

3.0 OBJECTIVES

The Overall goal of this work is to develop a rear-detection photothermal reflectance system to measure thermal diffusivity with high spatial resolution on micrometer-scale sample. The specific goals are:

- Build a theoretical model for rear-detection photothermal reflectance technique to optimize experimental setup.
- Make Sensitivity analysis and sample design.
- Do Experimental study with fused silica FIB sample ($11\mu m \times 18\mu m \times 2\mu m$).
- Determine experimental uncertainty.

4.0 THEORY DEVELOPMENT

The goal of this chapter is to develop an analytical model of frequency domain rear-detection photothermal reflectance technique. Existing 1D is introduced. However, it lacks consideration of several major issues may affect model's accuracy. An new model is carried out in this chapter. At last, the measurement sensitivity is analyzed.

4.1 Rear-Detection Photothermal Reflectance Technique (RDPRT)

The fundamental of RDPRT in frequency domain is to periodically modulate the intensity of heating laser and compare it with the corresponding in-phase temperature change of rear surface. The phase-lag profile carries the information of thermal properties of the sample. RDPRT can be solved in 1D and 3D models. Theoretically, a 3D model has higher accuracy than a 1D model since it takes 3D effect into consideration. However, the added complexity of a 3D model may greatly increase computation time, and sensitivity of desired parameter cannot be ensured. Notably, a 3D model requires multi-parameter inverse fitting process to extract desired parameters since it uses implicit analytical solution, which need spend a lot of time and uniqueness is hard to warrant [14]. It is found that the phase lag difference between 1D and 3D model is negligible in frequency range

applied to the thin plate sample geometry, because the design of the sample ensures near 1D heat transfer. Thus only 1D model is necessary for simulation and fitting.

4.1.1 Existing 1D model for single side FDPRT

1D FDPRT model has been used to solve tradition FDPRT, which applies heating and probe laser on same side. Several assumptions are made:

1) Infinite heating laser spot size. Thermal diffusion length is zero, which means total heat provided by heating laser is absorbed by surface.

2) The substrate layer is semi-infinite in both radius and depth directions.

3) The film layer is semi-infinite in radius direction.

4) Contact resistance caused by applying coating film at interface is zero.

Using FDPRT to measure thermal effusivity was reported successful by Yagi at el in 2004 [38]. The 1D model governing equations can be written as:

$$k_f \frac{\partial^2 T_f}{\partial x^2} - \rho_f c_f \frac{\partial T_f}{\partial t} = 0 \qquad 0 < x < h_1 \tag{4.1}$$

$$k_s \frac{\partial^2 T_s}{\partial x^2} - \rho_s c_s \frac{\partial T_s}{\partial t} = 0 \qquad h_1 < x < h_2 \tag{4.2}$$

where subscripts f, s, f represents front film, substrate, and rear film separately. h_1, $h_2 - h_1$, indicates the thickness of coating film and substrate separately.

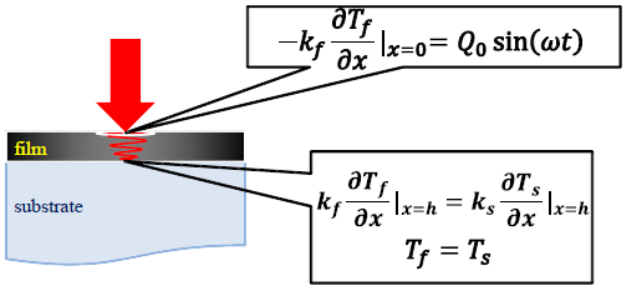

Figure 4-1 The layered model and boundary conditions of basic 1D model [43]

The Boundary condition at front surface is:

$$-k_{f1}\frac{\partial T_{f1}}{\partial t}\Big|_{x=0} = Q_0 \sin(\omega t) \tag{4.3}$$

The boundary conditions at interface of substrate are:

$$T_f\big|_{x=h} = T_s|_{x=h} \tag{4.4}$$

$$k_f \frac{\partial T_f}{\partial t}\Big|_{x=h_1} = k_s \frac{\partial T_s}{\partial t}\Big|_{x=h_1} \tag{4.5}$$

Then the phase-lag of the temperature response of probe laser to the heating laser can be written as:

$$-\delta = \frac{3}{4}\pi + tan^{-1}\left(\frac{cosh^2\sqrt{\frac{\omega T_f}{2}}(tanh\sqrt{\frac{\omega T_f}{2}}+\beta)(tanh\sqrt{\frac{\omega T_f}{2}}+\beta^{-1})}{cos^2\sqrt{\frac{\omega T_f}{2}}(\beta-\beta^{-1})tan\sqrt{\frac{\omega T_f}{2}}}\right) \tag{4.6}$$

where $\beta = e_s/e_f$, $\tau_f = h^2/D_f$.

Ideally, the 1D heating condition represents that the heat source is infinitely large, with uniform heat flux to heat the whole surface of a semi-infinite sample. But for the FIB sample applied in this study which is a slab with thickness of 2μm, the infinite-depth assumption cannot be satisfied. Also, for probe laser on sample rear surface, it is impossible

to assume infinite-depth since no signal could be detected on rear surface. Thus, a new model is needed for rear-detection frequency domain photothermal reflectance technique.

In Assumption 4, which assumes contact resistance is zero, R_{th} always exists at the interface between the film and substrate layer. Moreover, R_{th} can affects the thermal wave propagation significantly. Thus, another parameter needs to be applied to determine whether thermal contact resistance could be ignored:

$$\Omega_i \equiv k_i \sigma_{\mathrm{i}} R_{th} = (1 + \boldsymbol{i}) \frac{k_i R_{th}}{L_{si}} \tag{4.7}$$

where $L_{Ri} \equiv k_i R_{th}$ is a characteristic length accounting for thermal contact resistance. $1/R_{th}$ is 0.002~1.5MW/m^{2}K for Gas gap, and 1.5~1000MW/m^{2}K for real contact interface between two solid materials. $\gamma = L_{Ri}/L_{si}$ is used to determine whether thermal resistance need to be considered. If thermal conductance is not of interest, it is important to have $L_{Ri}/L_{si} \ll 1$. In this experiment, assuming $\frac{1}{R_{th}} = 200 MW/m^2K$, $L_{Ri}/L_{si} < 0.015$ in the frequency range of below 1MHz. Thus, it is safe to say that the interface thermal resistance can be ignored in this study.

In conclusion, a new 1D model need to be developed considering finite thickness and rear detection.

4.1.2 1D model for RDPRT using thermal wave method

The 1D model for a thin plate under harmonic heating of its front side is developed, with emphasis on DC temperature rise as well as the AC temperature oscillation. A DC-

biased sinusoidal intensity laser beam heats the sample and generates thermal wave propagating along the x direction normal to the surface as shown in Fig.4-1. The laser beam is considered to be spatially uniform with intensity modulation frequency f, and absorbed at the front surface ($x = 0$) where the 1-D heat flux is expressed by $\frac{F_0}{2}(1 + e^{i\omega t})$. The heat flux F_0 consists of two components, both with the amplitude of $F_0/2$: one is the constant flux (or DC bias) causing a time-independent temperature rise above the ambient, denoted by *R*, and the other is the harmonically oscillating heat flux (AC part) leading to a periodic temperature oscillation of the same frequency, denoted by *T*. The two components can be discussed separately, and the AC part heat flux is discussed first.

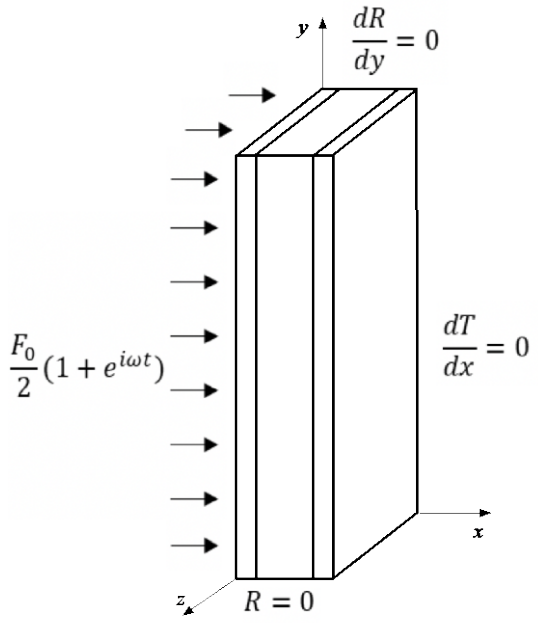

Figure 4-2 Heat transfer generated at y=0

The sample is designed to be a thin plate with micrometer in thickness (2 μm) and laterally large size ($11 \times 18\mu m$). It guarantees that the thermal wave generated by the harmonically oscillating heat flux can be treated as propagation only along the *x* direction which can be provided by that all the edges lie far enough to the heating laser beam comparing with thermal diffusion length [46]. For example, when the heating laser spot is located at the center of front surface and the modulate frequency is 100kHz, which thermal diffusion length is 1.7 μm, the sample's characteristic length in lateral direction is 3 times longer than the thermal diffusion length. It guarantees that 1D model can be applied. Heat conduction through the copper TEM grid holder and heat convection by air can also be ignored in the high frequency thermal waves model.

4.1.3 Thermal-wave (TW) field equation

Firstly, the conduction heat transfer equation can be written as:

$$\nabla^2 T(x,t) - \frac{1}{D}\frac{\partial}{\partial t}T(x,t) = -\frac{1}{k}Q(x,t) \tag{4.8}$$

Because the AC heating is periodic, and assuming that the temporal Fourier transform of T(x,t) exists,

$$\Theta(\mathrm{x},\omega) = \int_{-\infty}^{\infty} T(x,t)e^{-i\omega \mathrm{t}}dt \tag{4.9}$$

By taking Fourier transform of Eq. (4.8) and integration, wide-band field equation can be derived:

$$\nabla^2\Theta(x,\omega) - \sigma^2(\omega)\Theta(x,\omega) = -\frac{1}{k}Q(x,\omega) \tag{4.10}$$

Where σ is defined as $\sigma(\omega) \equiv (\frac{i\omega}{D})^{\frac{1}{2}} = (1+i)\sqrt{\omega/2D}$,it has the units m^{-1} and the physical meaning of a dispersive complex wave-number. By applying the Dirac delta function:

$$\delta(\omega - \omega_0) = \delta(\omega_0 - \omega) = \int_{-\infty}^{\infty} e^{-i(\omega-\omega_0)t} dt \tag{4.11}$$

The *complex thermal-wave-field equation* can be written as:

$$\nabla^2 T(x,\omega) - \sigma^2(\omega) T(x,\omega) = -\frac{1}{k} Q(x,\omega) \tag{4.12}$$

Which has single-spectral-component solution $T(r,\omega)$ to boundary-value problem associated with the TW field and within the frequency range of interest.

4.1.4 General solution for the thermal-wave (TW) field

Green's function approach is widespread and popular in solving wave field problems that have an arbitrary distribution heating source in space and time, as well as the initial and boundary conditions are inhomogeneous function of space and time. For diffusion-wave fields, the time dependence is harmonic, thus, the time variable can be eliminated and only boundary conditions need to be considered.

Here the wideband TW-field Green's function (Beck et al., 1992; Osizik 1980) is introduced:

$$\nabla^2 G(x|x_0;\omega;t_0) - \sigma^2(\omega) G(x|x_0;\omega;t_0) = -\frac{1}{k}\delta(x-x_0)e^{-i\omega t_0} \tag{4.13}$$

Combine (4.13) with (4.12), The *thermal-wave-field integral equation* can be yielded:

$$T(x,\omega) = \left(\frac{D}{k}\right) \iiint_{V_0} Q(x_0,\omega)\ \ G(x|x_0;\omega)\mathrm{d}V_0$$
$$+D \oint_{S_0} [G(x|x_0^s;\omega)\nabla_0 T(x^s,\omega) - T(x^s,\omega)\nabla_0 G(x|x_0^s;\omega)] \cdot d\boldsymbol{S_0} \tag{4.14}$$

In this equation, S_0 is the surface surrounding the domain volume V_0, which includes the harmonic source $Q(x,\omega)$. x_0^s is a coordinate point on $\boldsymbol{S_0}$, $d\boldsymbol{S_0}$, which indicates an infinitesimal vector in the outward direction normal to the boundary surface S_0: $d\boldsymbol{S_0} = \boldsymbol{n_0} dS_0$, with $\boldsymbol{n_0}$ being the outward unit vector.

As shown in Fig.4-2, an impulsive TW heating source is applied on front coating surface $\mathrm{x} = x_0 = 0$, and thermal conductivities and diffusivities are (k_i, D_i), i=1,2,3 representing front coating layer, sample layer and rear coating layer respectively. Because there is no heat source inside the substrate, function $H_2(x,x_0;\omega)$ and $H_3(x,x_0;\omega)$ are used to represent TW responses in sample and rear coating layer. The general solution of green's function and response functions are,

$$G(x|x_0;\omega) = \begin{cases} A_0 e^{\sigma_1 x_1} + A_1 e^{-\sigma_1 x_1}, 0 \le x_1 \le x_0 \\ A_2 e^{\sigma_1 x_1} + A_3 e^{-\sigma_1 x_1}, x_0 \le x_1 \le L_1 \end{cases} \tag{4.15}$$

$$H_2(x,x_0;\omega) = A_4 e^{\sigma_2 (x-L_1)} + A_5 e^{-\sigma_2 (x-L_1)}, \quad L_1 \le x_i \le L_1 + L_2 \tag{4.16}$$

and

$$H_3(x,x_0;\omega) = A_6 e^{\sigma_3 (x-L_1-L_2)} + A_7 e^{-\sigma_2 (x-L_1-L_2)},$$
$$L_1 + L_2 \le x_i \le L_1 + L_2 + L_3 \tag{4.17}$$

These field equations are subject to a set of boundary conditions and interfacial conditions:

$$\frac{d}{dx}G(x|x_0;\omega)\Big|_{x=x_0^+} - \frac{d}{dx}G(x|x_0;\omega)\Big|_{x=x_0^-} = -\frac{1}{D_1} \tag{4.18a}$$

$$G(x|x_0;\omega)|_{x=x_0^+} = G(x|x_0;\omega)|_{x=x_0^-} \tag{4.18b}$$

$$D_1\frac{d}{dx}G(x|x_0;\omega)\Big|_{x=x_0^+} = h_1 G(0|x_0;\omega) \tag{4.18c}$$

$$G(L_1|x_0;\omega) = H_2(L_1|x_0;\omega) \tag{4.18d}$$

$$D_1\frac{d}{dx}G(x|x_0;\omega)\Big|_{x=L_1} = D_2\frac{d}{dx}H_2(x|x_0;\omega)\Big|_{x=L_1} \tag{4.18e}$$

$$H_2(L_1+L_2,x_0;\omega) = H_3(L_1+L_2,x_0;\omega) \tag{4.18f}$$

$$D_2\frac{d}{dx}H_2(x|x_0;\omega)\Big|_{x=L_1+L_2} = D_3\frac{d}{dx}H_3(x|x_0;\omega)\Big|_{x=L_1+L_2} \tag{4.18g}$$

$$-D_3\frac{d}{dx}H_3(x|x_0;\omega)\Big|_{x=L_1+L_2+L_3} = h_3 H_3(L_1+L_2+L_3,x_0;\omega) \tag{4.18h}$$

From eight boundary and interfacial conditions above Eq. (4.18a) -(1.18h) , integration constants $(A_0,\cdots,A_7)$ can be derived by conventional means. The resulting Green's function in front surface is:

$$G(x|x_0;\omega) = \frac{1}{2\alpha_1\sigma_1\left(Z_3^{(2)}-R_1Z_3^{(1)}e^{-2\sigma_1L_1}\right)}\Big\{Z_3^{(1)}\left[e^{-\sigma_1[2L_1-(x+x_0)]}+R_1e^{-\sigma[2L_1-|x-x_0|]}\right]+$$

$$Z_3^{(2)}[e^{-\sigma_1|x-x_0|}+R_1e^{-\sigma_1(x+x_0)}\Big\} \qquad 0\le x\le L_1 \tag{4.19}$$

The impulse-response functions $H_2(x,x_0;\omega)$ and $H_3(x,x_0;\omega)$ can be written as:

$$H_2(x,x_0;\omega) = \frac{1}{\alpha_1\sigma_1}\left[\frac{e^{-\sigma_1(L_1-x_0)}+R_1e^{-\sigma_1(L_1+x_0)}}{Z_3^{(2)}-R_1Z_3^{(1)}e^{-2\sigma_1L_1}}\right] \tag{4.20}$$

$$\times\{X_{32}e^{-\sigma_2[(L_1+L_2)-x]}+Y_{32}e^{\sigma_2[(L_1+L_2)-x]}\} \quad L_1\le x\le L_1+L_2$$

and

$$H_3(x,x_0;\omega) = \frac{2}{\alpha_1\sigma_1}\left[\frac{e^{-\sigma_1(L_1-x_0)}+R_1e^{-\sigma_1(L_1+x_0)}}{Z_3^{(2)}-R_1Z_3^{(1)}e^{-2\sigma_1L_1}}\right] \tag{4.21}$$

$$\times\{e^{-\sigma_3[x-(L_1+L_2)]}+R_1e^{\sigma_3[2L-[x-(L_1+L_2)]}\} \quad L_1\le x\le L_1+L_2$$

where $Z_3^{(2)}$ and $Z_3^{(1)}$ are defined as three-layer coupling functions:

$$Z_3^{(2)} \equiv (1+b_{21})X_{32}e^{-\sigma_2 L_2} + (1-b_{21})Y_{32}e^{\sigma_2 L_2} \tag{4.22a}$$

$$Z_3^{(1)} \equiv (1-b_{21})X_{32}e^{-\sigma_2 L_2} + (1+b_{21})Y_{32}e^{\sigma_2 L_2} \tag{4.22b}$$

X_{32} and Y_{32} are two-layered coupling functions:

$$X_{ij} \equiv \left(1-b_{ij}\right) + R_i(1+b_{ij})e^{-2\sigma_i L_i} \tag{4.23a}$$

$$Y_{ij} \equiv \left(1+b_{ij}\right) + R_i(1-b_{ij})e^{-2\sigma_i L_i} \tag{4.23b}$$

X_{ij} and Y_{ij} are very useful in the thermal-wave physics of multi-layered model. b_{ij} and R_i are defined as:

$$b_{ij} = \frac{k_i\sigma_i}{k_j\sigma_j} \text{ and } R_i = \frac{k_j\sigma_j - h_j}{k_j\sigma_j + h_j}$$

The convection by air is ignored in this study, and R_i equals to 1.

The inhomogeneous boundary condition of the third kind resulting from a harmonic TW flux at the front surface (4.18a) can be written in the form:

$$-k_1 \frac{dT(0,\omega)}{\partial x}\Big|_{x=0} = \frac{1}{2}F_0 e^{i\omega t} \tag{4.24}$$

where $F_0 e^{i\omega t}$ is the AC part heat flux as mentioned before, the TW field is then related to the Green's function by:

$$\mathrm{T}(\mathrm{x},\omega) = -\mathrm{D}[G(x|x_0;\omega)\frac{d}{dx}\Theta(\mathrm{x}_0,\omega)\Big|_{x_0=0} \mathrm{T}(0,\omega)\frac{d}{dx}G(x|x_0;\omega)|_{x_0=0}]$$

$$= \frac{DF_0}{2k}G(x|0;\omega) \tag{4.25}$$

where the Green's function is (4.19), for the front coating layer, and the TW field can be written as:

$$\mathrm{T}(\mathrm{x},\omega) = \frac{D_1F_0}{2k_1}G(x|0;\omega)$$

$$= \frac{F_0(1+R_1)}{2k_1}\left[\frac{Z_3^{(1)}e^{-\sigma_1(2\delta_1-x)} + Z_3^{(2)}e^{-\sigma_1 x}}{D_1\sigma_1\left(Z_3^{(2)} - Z_3^{(1)}e^{-2\sigma_1\delta_1}\right)}\right] \tag{4.26}$$

For layer 2, 3, the TW field response layer equations (4.20), (4.21) can be written as following:

$$\mathrm{T}(\mathrm{x},\omega) = \frac{F_0}{4k_1\sigma_1}\left(\frac{(1+R_1)\left[e^{-\sigma_1 x}+\rho_{21}^{(3)}e^{-\sigma 1(2L_1-x)}\right]}{1-R_1\rho_{21}^{(3)}e^{-2\sigma_1 L_1}}\right) \tag{4.27}$$

where the definition of $\rho_{21}^{(3)}$ depends on the number of layers, and the schematic cross section is shown in Figure 4-3:

$$\rho_{21}^{(3)} = \frac{(1-b_{21})+\rho_{32}^{(3)}(1+b_{21})e^{-2\sigma_2 L_2}}{(1+b_{21})+\rho_{32}^{(3)}(1-b_{21})e^{-2\sigma_2 L_2}} \tag{4.28}$$

$$\rho_{32}^{(3)} = \frac{(1-b_{32})+R_3(1+b_{32})e^{-2\sigma_3 L_3}}{(1+b_{32})+R_3(1-b_{32})e^{-2\sigma_3 L_3}} \tag{4.29}$$

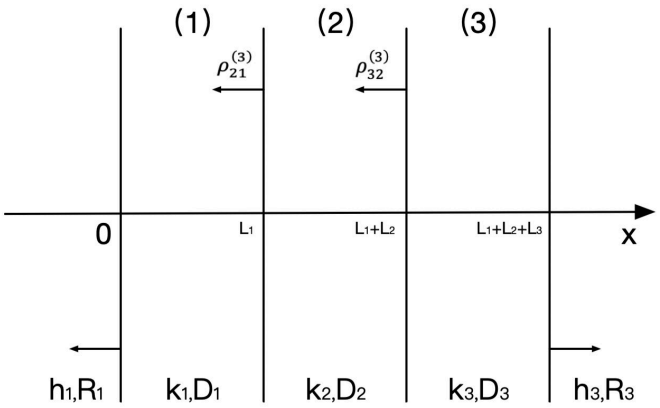

Figure 4-3 Schematic of cross section of 3-layer sample

The magnitude of thermal wave field is given by $|\mathrm{T}(\mathrm{x},\omega)|$, and the phase is obtained from:

$$\varphi = tan^{-1}\left(\frac{Imag(T)}{Real(T)}\right) \tag{4.30}$$

In this study, the AC temperature at the rear surface is defined as $T_r = T(L_1 + L_2 + L_3)$, then the amplitude and phase of rear surface can be written by $|T_r|$ and φ_r respectively. Figure 4-4 shows a simulation result of φ_r in frequency domain.

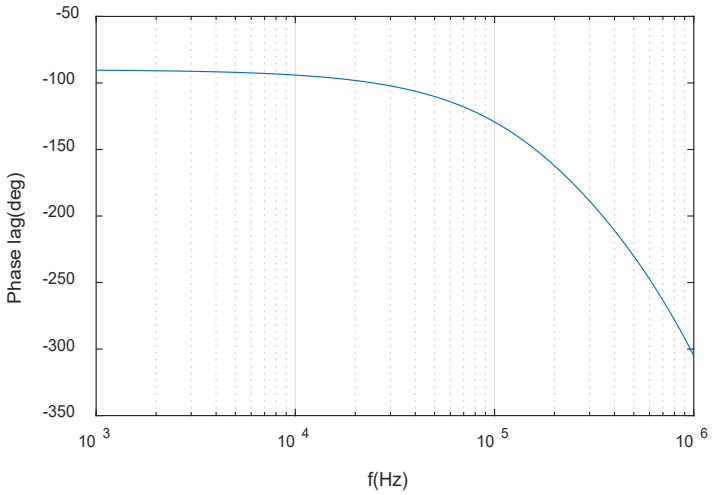

Figure 4-4 Simulation result of RDPRT

4.2 Coating and Sensitivity Analysis

Sensitivity analysis is a useful method for experiment design and data processing. High sensitivity to a certain desired parameter is wanted. Because the relative high sensitivity of one parameter would reduce other low-sensitivity parameter uncertainty propagation. In general, the sensitivity is defined as:

$$S(\xi) = \frac{\varphi(\varepsilon+\Delta\varepsilon)-\varphi(\varepsilon)}{\Delta} \tag{4.31}$$

where ε is the parameter to be investigated, Δ is the relative change of the parameter, it is set as 0.01 in this study. The mathematical meaning of this sensitivity definition is the change of phase φ caused by the parameter ε increases 100%.

The sensitivity analysis is first performed on a sample without coatings to focus on the physics without complex math. Without consideration of coating layers, which means L_1=L_3=0, the 1D thermal wave field can be expressed in a much simpler form:

$$T(0 \le x \le L_2) = \frac{F_0}{2k_2L_2}\frac{e^{-L_2x} + e^{-\sigma_2(2L_2-x)}}{1 - e^{-2\sigma_2L_2}} \tag{4.32}$$

Then the AC temperature at the rear surface of lamella sample is written as:

$$T_r = \frac{F_0L_{th}}{k_2(1+i)}\frac{e^{-(1+i)L_2/L_{th}}}{1 - e^{-2(1+i)L_2/L_{th}}} \tag{4.33}$$

It is found that the phase-lag φ (defined in 4.30) is only dependent on the ratio L_{th}/L_2 as shown in Eq. (4.33). Thus, thermal wave length normalized by the sample thickness is used as a dimensionless quantity to relate the modulation frequency to the thickness for further analysis.

For thermoreflectance measurements, the lower bound of the AC temperature amplitude is usually in the range of 0.5~2.5K, and thermal wave length should be similar to the sample thickness in order to achieve a detectable and sensitive phase measurement. From Eq. (4.34), the heat flux required to generate $|T_r|$ can be written as:

$$F_0 = \frac{\sqrt{2}k_2}{L_{th}}\left|\frac{1 - e^{-2(1+i)L_2/L_{th}}}{e^{-(1+i)L_2/L_{th}}}\right||T_r| \tag{4.34}$$

Under the conditions of $L_{th} = L_2 = 2\mu m$ and k_2=1W/Km, $|T_r|$ of 0.5K requires the heat flux amplitude as much as 2×10^6W/m^2. For an area of 10x20 □m^2, the corresponding power need is 0.4 mW.

As aforementioned, phase φ is only dependent on the ratio L_{th}/L_2. Thus, it is necessary to investigate the sensitivity of the ratio. As shown in Fig.4-5, when increasing L_{th}/L_2, the sensitivity of diffusivity D_2 begins to drop. It is known that $L_{th} \equiv \sqrt{\frac{D_2}{\pi f}}$, thus, to maintain high system sensitivity to the desired parameter D_2, high frequency is needed.

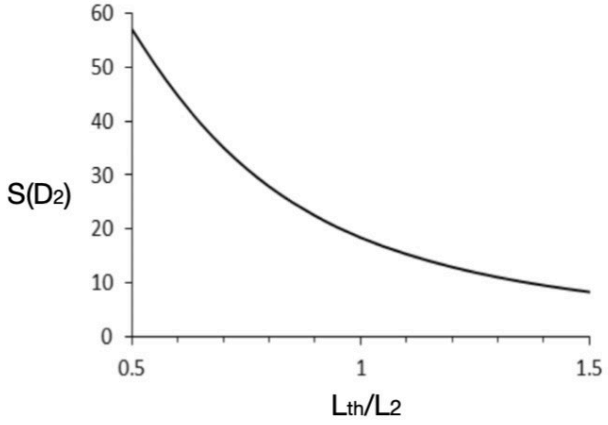

Figure 4-5 Sensitivity of thermal diffusivity of the sample without coating

However, increase frequency would shorten L_{th}, which means shorten the penetration depth of thermal wave, and weaken temperature oscillation at the rear surface. Thus, it is necessary to find the relation between $|T_r|$ and L_{th}/L_2. When setting heating laser power is 0.8mW, The AC temperature amplitude at the front and rear surfaces to L_{th}/L_2 is plotted in Fig.4-6. It shows that the temperature amplitude of front surface $|T_0|$ is always

greater than 0.5K when $L_{th}/L_2 > 0.5$; For rear surface, L_{th}/L_2 should be greater than 0.7 to guarantee $|T_r| > 0.5$.

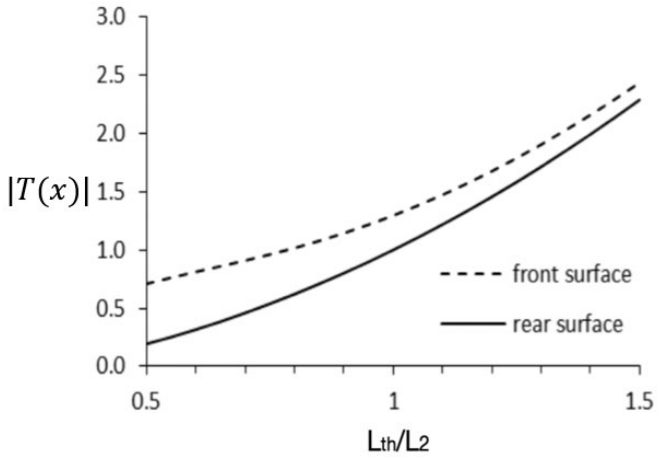

Figure 4-6 Relation between $|T(x)|$ and L_{th}/L_2 without coating

Increase the heating laser intensity is another method to increase $|T(x)|$. However, it is found that increasing F_0 would not only increase the maximum DC temperature on sample—cause coating surface melting—but also enlarge the DC temperature gradient inside the sample.

Thus, it is also necessary to take the DC temperature rise in sample into consideration, since it is important for setting proper heating laser power in experiment. The DC temperature rises of sample is analyzed separately from AC thermal wave. The constant heat flux increases the temperature of the sample, and the heat will dissipate into the copper substrate. Because the thin plate sample applied in this paper is thin enough, it is safe to assume an identical temperature for all height along the x direction, which normal to the

surface. The DC temperature rise under the thermally thin assumption is described by a 1D fin conduction equation:

$$\sum k_i D_i \frac{d^2R}{dy^2} = \frac{F_0}{2} \tag{4.35}$$

Subjected to the boundary conditions:

$$\frac{dR(y=H)}{dy} = 0 \tag{4.36}$$

$$R(y=0) = 0 \tag{4.37}$$

Because of the good thermal contact of the sample with its copper substrate, the temperature rise is imposed as zero at $y = 0$. Combining boundary conditions, (4.36) could be solved:

$$R(y) = \frac{F_0}{2\sum k_i L_i}\left(H - \frac{y}{2}\right)y \tag{4.38}$$

where H is the height of sample. It can be found that the DC temperature rise has a half parabolic profile along the y direction. The highest temperature appears at the free end of the sample:

$$R_{max} = R(y=H) = \frac{F_0 h^2}{4\sum k_i L_i} \tag{4.39}$$

Now considering AC thermal wave and DC temperature rise together. Because high $|T_r|$ and low R_{max} are desired at the same time, another dimensionless number, $\frac{R_{max}}{|T_r|}$ is introduced in this study to investigate relation between these two parameters.

$$\frac{R_{max}}{|T_r|} = \frac{\sqrt{2}(H/L_2)^2}{4L_2/L_{th}}\left|\frac{1 - e^{-2(1+\boldsymbol{i})L_2/L_{th}}}{e^{-(1+\boldsymbol{i})L_2/L_{th}}}\right| \tag{4.40}$$

From (4.41) it can be found that $\frac{R_{max}}{|T_r|}$ is dependent on L_{th}/L_2, but not the heat flux intensity. As we known that high frequency is preferred to achieve high sensitivity on

thermal diffusivity, however, by considering (4.41), increase frequency would decrease L_{th}/L_2,which would lead to increase $\frac{R_{max}}{|T_r|}$, then cause larger DC temperature gradient for fixed $|T_r|$. For example, when $|T_r|$ is in the detectable range of 0.5~2.5K, R_{max} could be 200 to 400 times larger than $|T_r|$ in low L_{th}/L_2 region. Under this occasion, the DC temperature rise might damage the sample.

From above analysis, an optimized solution should have high AC temperature amplitude $|T_r|$ and low DC temperature R_{max}. In this paper, metallic coating is chosen to provide better experimental conditions. Metallic coating on front and rear surfaces of sample would affect heat transfer in several ways. Firstly, the coating would add more cross-sectional path for heat conduction to the substrate. According to Eq. (4.40), the R_{max} would drop significantly by ratio $\frac{\sum k_i L_i}{k_2 L_2}$. Secondly, proper coating has a high thermoreflectance coefficient at probe laser wavelength, which could ensure good signal sensitivity. Thirdly, coating with a high thermal reflectivity could also guarantee good reflected signal intensity and can keep DC temperature rise of the surface low. However, the coating would create additional phase lag of thermal wave, and may increase the measurement uncertainty. Sensitivity of coating layer is discussed later in this chapter.

In this paper, high thermal conductivity coating material are applied (gold, k = 100W/Km, D= 42.36mm^2/s) on fused silica sample (k = 1.38W/Km, D= 0.89mm^2/s). The ratio of $\frac{R_{max}}{|T_r|}$ is significantly reduced with the addition of gold film. For example, $0.2L_2$ thickness of gold coating film would decrease $\frac{R_{max}}{|T_r|}$ by a factor of 10, regardless of surface

side. Gold coating would also reduce R_{max} greatly because of its high thermal conductivity in y-direction but has negligible influence on thermal wave in x-direction.

Table 4-1 The Parameters used in sensitivity analysis

Parameter	Unit	Front coating	sample	Rear coating
K	$W \cdot \mathrm{m}^{-1} \cdot K^{-1}$	9.6	1.38	316
D	m^2/s	4.07e-6	0.876	1.27e-4
Thickness	μm	2.16	80e-3	120e-3
Spot size	μm	15	-	-

The main objective of this sensitivity analysis is to find the suitable frequency range for extracting the desired parameter, thermal diffusivity. Other thermal properties as well as thickness of each layer are considered. The result is plotted in Fig.4-6 to 4-8. Parameters used in the sensitivity analysis are listed in Table.4-2.

As shown in Fig.4-7, 4-8 it can be found that S(ξ) has most sensitivity on thermal diffusivity of substrate layer in frequency region lager than 5×10^4Hz, which is expected. Thus, it is safe to say that extracting thermal diffusivity of substrate layer in inverse fitting process with high accuracy is possible, but high frequency is required.

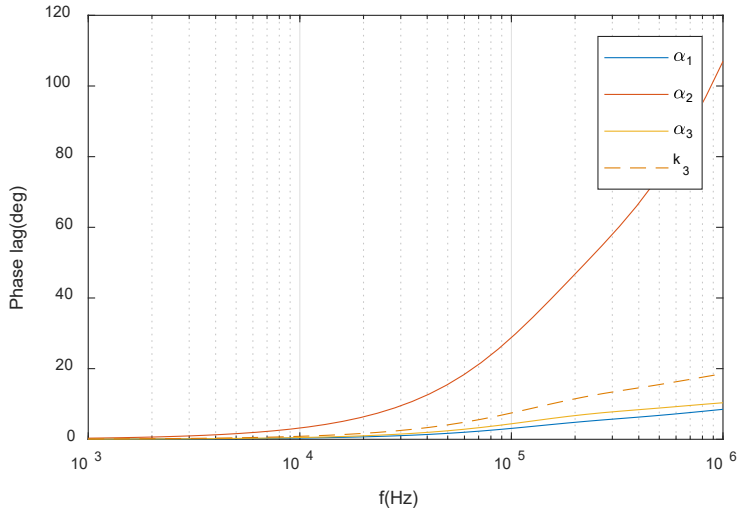

Figure 4-7 Sensitivity analysis comparing diffusivity and conductivity of each layer

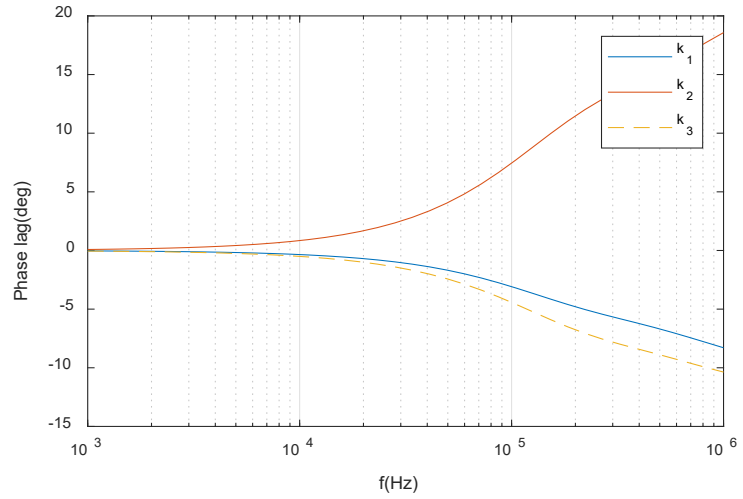

Figure 4-8 Sensitivity analysis comparing conductivity of each layer

In Fig.4-9, it can be found that the thickness of sample layer has high sensitivity in all frequency regions, in the other words, the thickness of substrate layer is very important to the experiment precision while precise thickness of front and rear coating layer is not important.

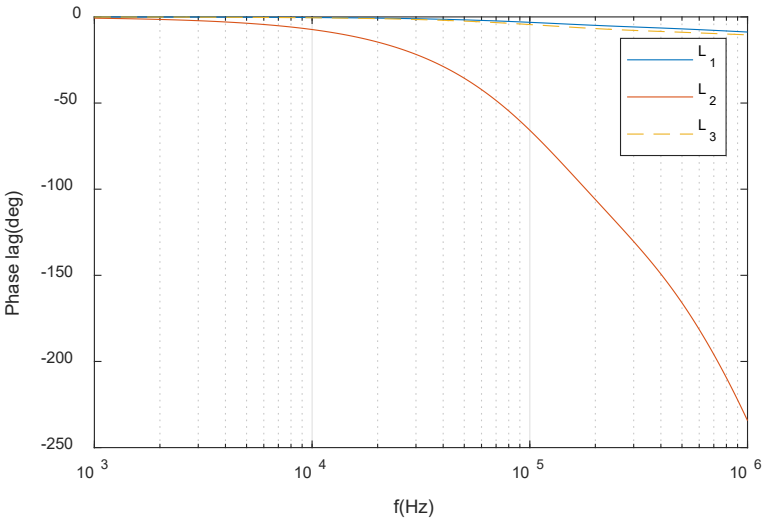

Figure 4-9 Sensitivity analysis comparing thickness of each layer

5.0 EXPERIMENT PROCEDURE

In Chapter 5, the design and build of RDPRT experiment platform is presented, sample preparation is also discussed subsequently.

5.1 Experiment Setup

Different from tradition FDPRT, rear-detection FDPRT requires heating laser and probe laser spot on front and rear surface separately, the design drawing is shown in Fig.5-1. The wavelength of two continuous-wave lasers are 532nm (Laser quantum GEM 532, green's light) and 671nm (lab built, red light), and the maximum power output are about 500mW and 200mW separately. Green's laser is used as probe laser, and red laser is used as heating laser, which decides the coating materials on front and rear surface.

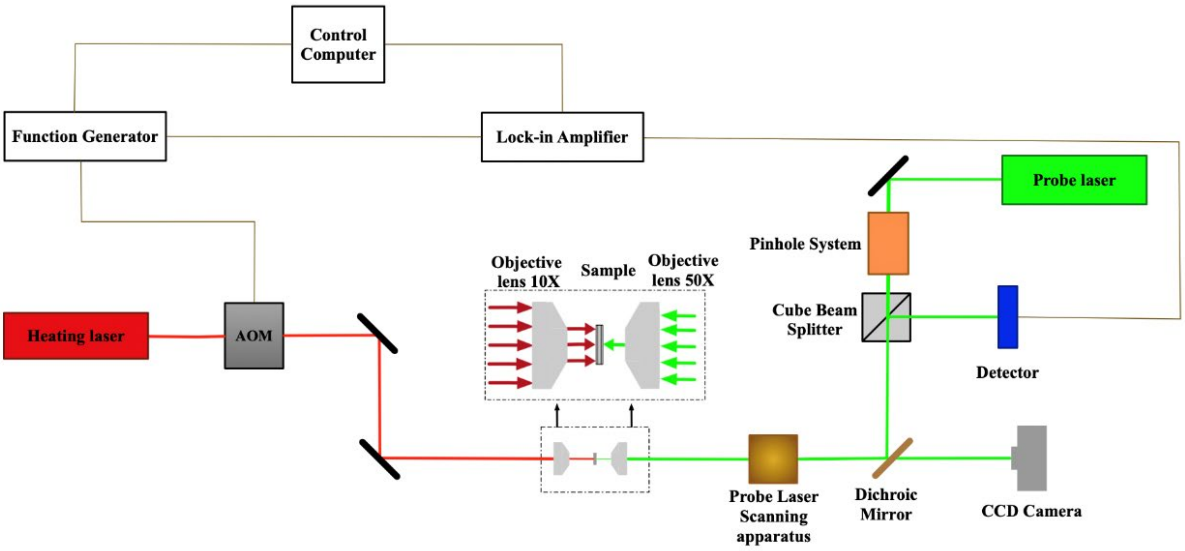

Figure 5-1 Design diagram of experiment setup

As we can see in Fig.5.1, on heating laser side, the heating laser would pass an acousto-optic modulator (AOM, G&H, model R35085-3 with the driver model N21080-1SAS) first, which is applied to modulate the amplitude and frequency of heating laser. AOM is controlled by a function generator (Agilent Technologies model 33220A). After AOM, the heating laser beam passes a pair of reflective mirrors and irises, two same height level Irises are applied to set the standard height level of the heating laser path. If the heating laser can pass through the center of both irises, then the heating laser can be guaranteed to be horizontal on a millimeter-scale. A 10X objective lens (Nikon, SLWD 10X) is used at last to increase the energy intensity and focus the heating laser to appropriate spot size.

On probe laser side, several reflective mirrors and irises are applied to orient the probe laser path like the heating laser. A 50:50 visible non-polarizing Beam splitters cube (Thorlabs, BS010) is added to split the reflected probe laser beam. The reflected probe

beam is then sent into the photodetector (New Focus model 1621) and analyzed by a lock-in amplifier (Stanford Research System model SR830). Between the photodetector and the beam splitter cube, a band pass filter is used to ensure no heating laser energy reaches photodetector, which could increase the uncertainty of the measurement. To improve the probe laser quality and reduce noise, a pinhole system is also used, which consists of two plano-convex lens (LA1805-A and LA1608-A separately) and a pinhole (national Aperture 1-40+M-1). The existence of noise in probe laser is due to Gaussian beam, which has a self-contained spatially varying intensity "noise". When the beam is focused by an aspherical lens, the input beam is transformed into a central Gaussian spot (shown in Fig.5-2). The radial position of the side fringes is proportional to the spatial frequency of the "noise" [Thorlabs pinholes].

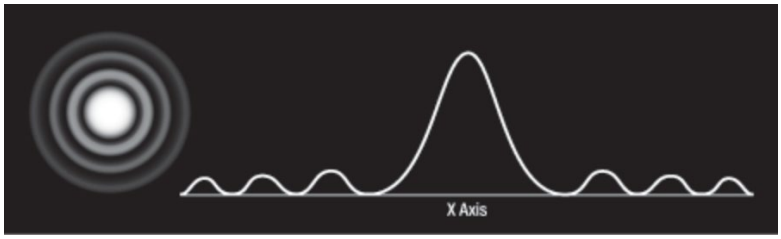

Figure 5-2 Input Gaussian beam

By using a pinhole system, it can "cut off" the noise part and output a clean Gaussian beam (see Fig.5-3 below).

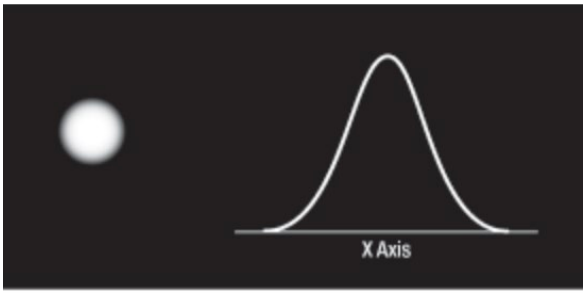

Figure 5-3 Output clean Gaussian beam

Because the front area of the sample is $11 \times 18\mu m$, it is hard to use manual adjustment to control the probe laser spot position in micrometer-scale, thus, a pair of confocal lenses and motorized stage are applied to solve this problem. The first confocal lens is mounted on the motorized stage (Newport model VP-25XA), a dichroic filter is also mounted on motorized stage which has high reflectivity (above 99%) over probe laser wavelength, and high transmittance over heating laser wavelength (99%). The latter characteristic is also an important requirement which avoids too much heating laser energy from going into the photodetector. The probe laser passes second confocal lens, which has fixed position. The probe laser then passes a 50X objective lens (Nikon SLWD) and reaches sample's rear surface with a spot diameter about $1\,\mu m$, which satisfies the requirement of high spatial-resolution. A CCD camera with micrometer-resolution is used to help check the position of both heating and probe laser on sample.

The experimental setup is given in Fig.5-4.

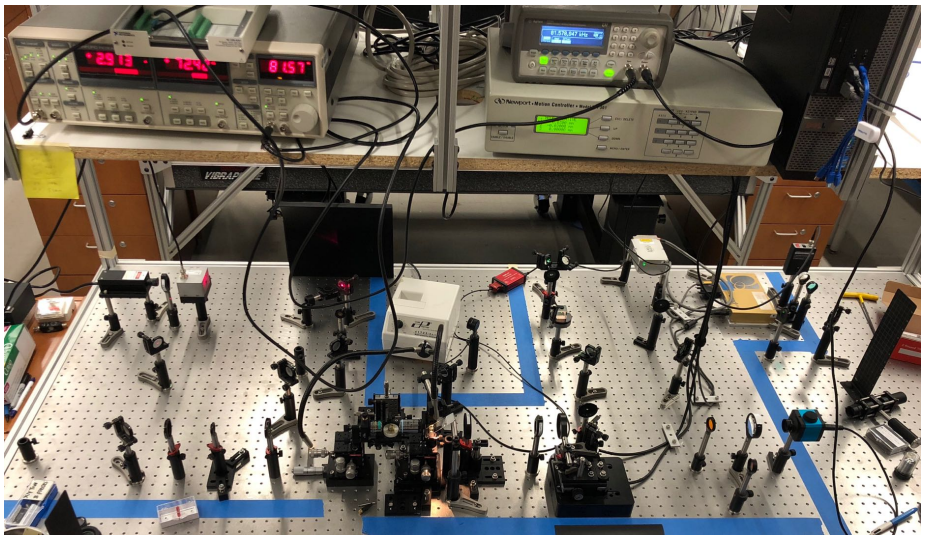

Figure 5-4 Experiment setup

5.1.1 Description of sample

The size of validation sample is $(11 \times 18 \times 2)\mu m$, fused silica has been selected to be the sample material to represent highly burnt nuclear fuel as they have similar thermal conductivity ($1.4\ W \cdot m^{-1}K^{-1}$). The sample is mounted on Copper TEM grids by platinum using FIB fabrication technique, shown in Fig. 5-3 a). The front and rear surface of sample are well parallel to each other within $\pm 1\%$. Two reference sample are made, the first reference sample is a Glass slide with gold coating. It is used to do pre-test and orient laser path. The second reference sample is made of fused silica, the validation sample is cut off from this reference sample to guarantee same thermal properties and is coated with gold on front surface and titanium on rear surface. The reference sample is coated with validation sample simultaneously to guarantee same coating condition, for identical

thickness of front and rear coating. This identical coating reference sample is important to acquire thermal parameters of front and rear coating layers, which will be discussed next. The specifications of the validation sample are summarized in Table 5-1.

Table 5-1 Specifications of the validation sample

Coating layer	Gold	Fused silica	Titanium
k $[\mathrm{W} \cdot m^{-1} \cdot K^{-1}]$	316	-	9.6
D [m^2/s]	1.27×10^{-4}	-	4.07×10^{-6}
L[nm]	80	2.16×10^{3}	120

In Fig.5-5: a) the optical microscopy image for the sample mounted on a TEM Copper grid by platinum soldering. b) and c) SEM images for the front and side view of the sample before coating: length × width is 18.3 μm ×11.2 μm, thickness is 2.16±0.03 μm varying within 1% from the base to the free end.

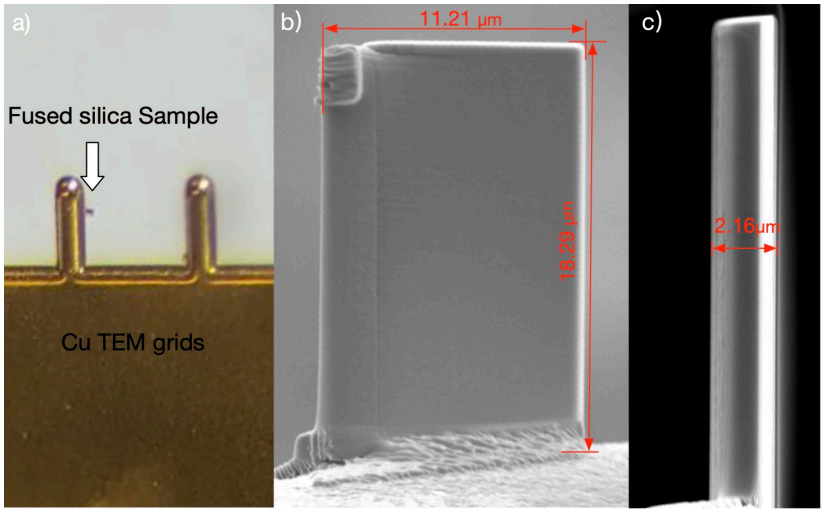

Figure 5-5 Image of the FIB fabricated fused silica sample.

Titanium is selected as the front surface coating material because of its good thermal absorptivity at heating laser wavelength (671nm), which ensures the sample receives good heating energy intensity. Fig.5-6 shows the titanium coating on front surface.

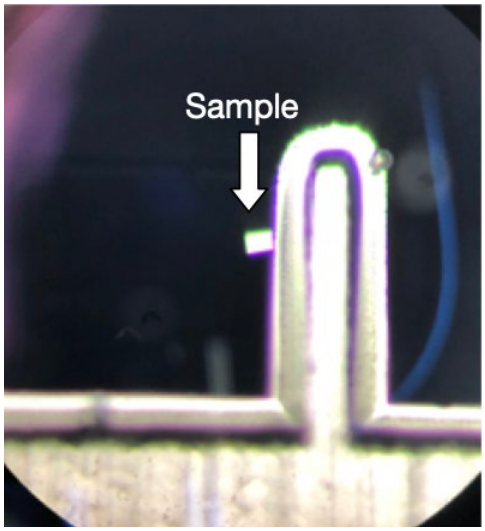

Figure 5-6 500× magnified image of sample rear side with ~95 nm thick Titanium coating

Gold is selected as the rear surface coating material since gold has a high thermoreflectance coefficient ($-3 \times 10^4 K^{-1}$) at probe laser wavelength, which ensure good signal sensitivity. Gold also has high thermal reflectivity which guarantees good reflected signal intensity and can keep surface from overheating since the energy density of probe laser is large after pass the 50X objective lens. Fig.5-7shows the gold coating on rear surface.

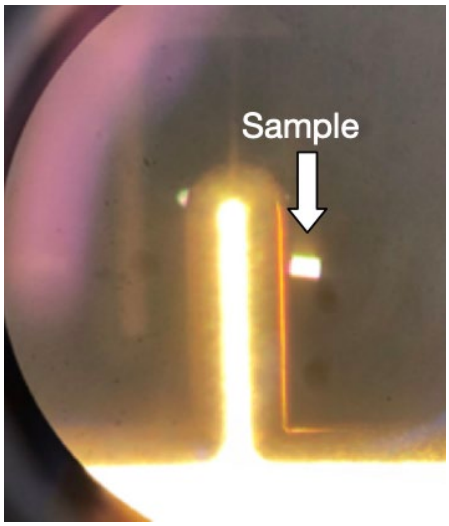

Figure 5-7 500× magnified image of sample front side with ~120 nm thick gold coating

5.2 Experimental Procedure

The experiment procedure should follow the method in Chapter 4, as previously mentioned. Several other thermal parameters of front and rear coating layers, including

thermal conductivity D_1, D_3 and thermal conductivity k_1 and k_3 are required. Those parameters can be acquired by traditional FDPRT and SDPRT methods.

From sensitivity analysis in Chapter 4, it is also known that high frequency heating is preferred to get D_2, and an inverse fitting process is required. It is worth noting that because of characteristic of thermal diffusion length $L_{th} \equiv \sqrt{\frac{D_2}{\pi f}}$, the thermal wave propagation would attenuate exponentially with increasing frequency, which would also decrease the temperature oscillation in the rear surface and cause large measurement uncertainty. In consideration of above requirements, the frequency region of heating laser is chosen to be from 30k to 200kHz.

Because the Gaussian distribution of the heating laser, the energy density would drop significantly along with radius direction. Thus, it is necessary to focus the center of the heating laser concentric with center of the probe laser to guarantee maximum heat wave amplitude in rear surface. A CCD camera is employed to monitor both heating laser and probe laser position. It allows that the heating laser and the probe laser spots can be seen simultaneously, small adjustment can be made by the motorized stage until center of both laser spots coincide. By using this method, the precision could reach micro-meter level. A better way to optimize concentric-ness can be done by using Lock-in Amplifier. Reading the amplitude signal and adjusting motorized stage at same time, a maximum amplitude signal can be found. High precision can be achieved using this method.

6.0 EXPERIMENT RESULT AND DISCUSSION

In this chapter, the experimental results are given and discussed. All steps follow the procedure introduced in Section 5.3: the rear-detection PRT is applied in frequency region 50k to 200kHz. Thermal diffusivity is extracted from the phase lag profile, then compare it with the value given by vendors. Sources of uncertainty are discussed, and a quantitative uncertainty analysis is carried out in the end of this chapter.

6.1 Parameters of Coating Films

As aforementioned, thermal parameters of front and rear coating films are obtained from reference sample by traditional FDPRT and SDPRT methods. The thickness of front and rear coating films on the reference sample are measured by a profilometer. From sensitivity analysis in Chapter 4, it is found that the thickness of front and rear coating film has limited effect on the phase lag, and the thermal conductivity of the coatings also has little impact on phase lag as well. They all show one order of magnitude less sensitivity compare to the sample thermal diffusivity, D_2. The measurement results are summarized in Table 6-1.

Table 6-1 Parameters of front and rear coating film

Coating layer	Gold	Titanium
k $[\mathrm{W} \cdot m^{-1} \cdot K^{-1}]$	316	9.6
D [m^2/s]	1.27×10^{-4}	4.07×10^{-6}
L[nm]	80	120

6.2 Experiment Procedure

The RDPRT measurement is carried out in high frequency region, reference sample 1 is applied to orient light path to guarantee concentric of heating laser spot and probe laser spot. 50X long-working distance objective lens is used to focus probe laser to radius of 2 μm, 10X objective lens is used to focus the heating laser to radius around 20μm. It should be noted that the heating laser is not well-focused by 10X objective lens on purpose, the reason is for heating to be near uniform on the whole front surface. 20 scan frequency points are applied from 50k to 200kHz, and 10 times repetition at each frequency point.

6.3 Experimental Result

Before extract diffusivity from phase data, the useful frequency range of data needs to be found. Fig.6-1 shows the 3 full series of data from 10k to 200kHz. The thermal diffusivity at each frequency point is calculated in the frequency range starts from the point frequency to 200kHz. For example, thermal diffusivity at 50kHz is extracted from frequency range from 50k to 200kHz; at 100kHz is extracted from frequency range from 100k to 200kHz. As we can see in the Fig.6-1, points start with frequency smaller than 50kHz are scattered. This is because when frequency is smaller than 50kHz, thermal diffusion length L_{th} would be larger than 2.4 μm, which leads to increasing edge effect. In the frequency region from 50kHz to 100kHz, the obtained thermal diffusivity shows acceptable fluctuation. When starting frequency is larger than 100kHz, the fitting results become scattered again due to insufficient data points. Thus, 50kHz to 200kHz is chosen to be the appropriate frequency range for data fitting.

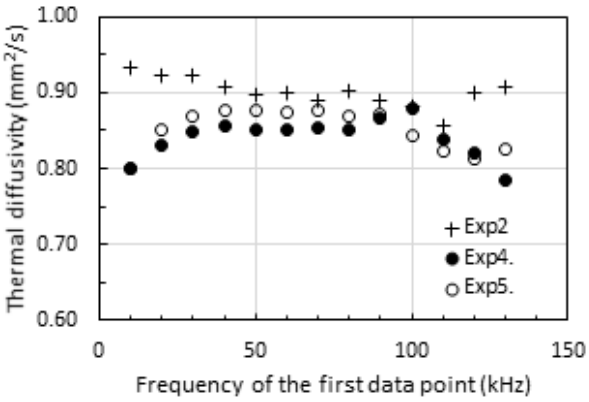

Figure 6-1 Frequency range analysis of RDPRT

One typical series of RDPRT experimental data is plotted in Fig.6-2, the interval of scan frequency is 10kHz, for 20-points from10kHz to 200kHz. Least-squares fitting method is applied to generate a best-fit curve from data range from 50kHz to 200kHz. It is apparent that data points at frequency 10kHz and 20kHz deviate from the best-fit curve, which shows that the edge effect increases uncertainty in low frequency range. Thermal diffusivity is fitted from four sets of experimental data: 0.896, 0,849, 0.875 and 0.884 mm^2/s. The average value of thermal diffusivity can obtained :0.876 mm^2/s, which shows good agreements to literature value, 0.891 mm^2/s ,with less than 2% error.

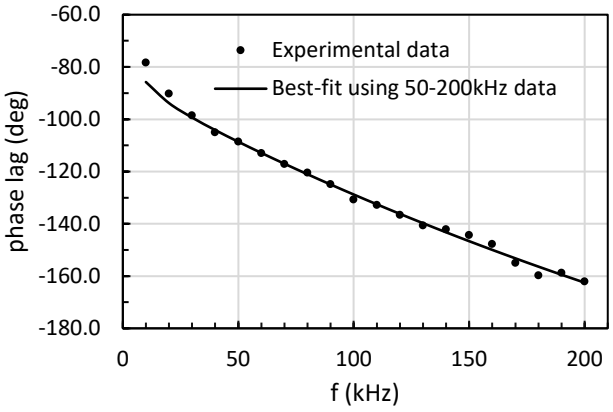

Figure 6-2 Experimental data and fitting curve

6.4 Uncertainty Analysis

In this section, main uncertainty sources are listed, and their contribution to the final uncertainty are summarized in Table. 6-2. The uncertainty to all thickness is obtained by fitting the experiment data with their lower or upper bound. For example, the roughness of front and rear coating is 15nm, and if setting 105 nm as the thickness of Au coating, then the fitted thermal diffusivity is less by 1.6%. The experiment noise, which includes cables and frequency response error of AOM and photodetector, leads to 0.5 to 2.5-degree fluctuation of phase, and causes 2% uncertainty. The Gaussian beam with waist radius of $35\mu m$ would increase the uncertainty of diffusivity 2%. As a result, the overall uncertainty of thermal diffusivity of the sample is with 6%, and the majority is attributed to the roughness of all layers. The details are listed below.

1) Film thickness. Thickness of coatings of the reference sample is measured by a surface profilometer. From measurement it is found that the surface roughness of Ti coating and Au coating is 15nm. This roughness would cause uncertainty as explained previously. The thickness of the fused silica layer on validation sample is measured by the SEM image, ±0.03 □m fluctuation of thickness is found.

2) Experimental noise from cables. From test it is found that BNC cables could generates uncertainty, which is caused by electrical signal interference and has positive correlation with heating laser's frequency. Although the phenomenon is inevitable, there

are several solutions to suppress it: use high quality cable which can shield signal interference from other source; choose cable as short as possible.

3) Experimental noise from frequency response error of AOM and photodetector: AOM has a late-response phenomenon, which would cause undesired fluctuation of phase lag. The effect of late-response of AOM has linear relation with heating laser frequency as well. A possible solution to reduce uncertainty sources (3), (4) is represented below. At each frequency, when the standard experiment procedure is followed, the amplitude and phase lag data can be combined and defined as data vector. By blocking probe laser to the photodetector, a weak data vector can be recorded, which is the pure background noise vector generated by the sources (3), (4). The sum of desired data and error (3), (4) can be obtained by reading data following the standard experiment procedure. By subtracting the background noise from data, the sum of phase fluctuation caused by (2) and (3) is 0.5 to 2.5 degree for frequency range 50k to 200kHz, and cause $\pm$2% uncertainty. They are called experimental noise.

4)Heating laser beam: as mentioned before in Section 5.1, the heat laser system generates a Gaussian beam with waist radius of 35μm at sample front surface. The heating laser cannot provide ideal uniform 1D heat flux condition, and would cause uncertainty by 2%. This value is obtained from comparing the 1D model to 3D model in MATLAB.

The summary of the main uncertainty sources is concluded in Table.6-2. As a result, the overall uncertainty of thermal diffusivity of the smaple is within 6%, and the majority is attributed to the uncertainty of thickness of all layers.

Table 6-2 Uncertainty sources

Sources	Designed model	Experimental conditions	Uncertainty of D
Thickness of SiO_2	2.16μm	±0.03μm	±2.8%
Thickness of Au film	120nm	±15nm	±1.6%
Thickness of Ti film	80nm	±15nm	±1.6%
Experimental noise	-	0.5-2.5deg at 50-200kHz	±2%
Gaussian heating laser	Uniform	Gaussian of 35μm in waist radius	2%

7.0 CONCLUSION AND FUTURE WORK

7.1 Conclusions

Based on photothermal reflectance method, a thermal diffusivity measurement technique and system for solid micrometer-sized plate sample was developed. This study uses a rear detection approach to expand the applicability of thermal wave technique to low thermal conductivity materials. Different from conventional photothermal reflectance method, the thermal wave is detected at the opposite surface to simplify the beam size control and alignment. An analytic model was established for the heat transfer process, including the consideration of DC temperature rise of the sample. The analysis shows that special coating is needed for sample to suppress DC temperature rise as well as to generate enough AC temperature amplitude on rear surface. Ti is found to be the proper front coating material and Au is found to be the proper rear coating material. The experimental setup was optimized for measuring a SiO_2 sample, which could represents low thermal conductivity material or irradiated nuclear fuel, of 2.16 μm × 11.2 μm × 18.3 μm coated with 95 nm Ti film on the front surface and 120 nm Au film on the rear surface.

50kHz to 200kHz is chosen to be the suitable experiment frequency range considering sensitivity analysis and experiment conditions. Phase lag data is read by Lock-in Amplifier and inverse fitting method is applied to extract thermal diffusivity from data. The average

value of thermal diffusivity is obtained to be 0.876 mm^2/s, which shows good agreements to literature value, the overall uncertainty is within 6%. Main uncertainty sources include roughness in coating films, baseline electric noise, frequency response error of photodetector and Gaussian heating beam.

This technique can be used to determine thermal diffusivity of samples of micrometers in size, such as Focus Ion Beam lift off samples. The small sample size can minimize sample radiation of nuclear materials and achieve high spatial resolution for local thermal property determination.

7.2 Future Work

1) For current RDPRT, system optimization will be needed if the sample is known to have a high thermal conductivity (greater than $10\mathrm{W} \cdot m^{-1} \cdot K^{-1}$).

2) In order to provide measurement setup mobility, optical fiber could take place of current lab-build laser system, which can simplify the light path greatly and ease the system maintenance.

3) Point to point heating technique is under studying, which requires 3D thermal wave model. High melting temperature of front coating and high quality of heating laser need to be considered.

BIBLIOGRAPHY

[1] A. Mandelis, 2013, *Diffusion-Wave Fields: mathematical methods and Green's functions*. Springer Science & Business Media.

[2] R. Berman, 1976, *Thermal conductivity in Solids*, Clarendon, Oxford.

[3] F. Incropera, D. Dewitt, T. Nergman and A. Lavine, 2006, *Fundamentals of Heat and Mass Transfer*, John Wiley & Sons Inc, Hoboken, NJ.

[4] H.S. Carslaw and J.C Jaeger, 1959, *Conduction of Heat in Solids* (2nd ed.), Oxford University Press, London.

[5] N. Burger, A. Laachachi, M. Ferriol, M. Lutz, V. Toniazzo and D. Ruch. 2016, "Review of Thermal Conductivity in Composites: mechanisms, parameters and theory," Polymer Science.

[6] W.D. Callister, 2007, *Materials Science and Engineering: an introduction*, John Wiley & Sons Inc., New York.

[7] H. F. Bowman, E. G. Cravalho and M. Woods, "Theory, Measurement, and Application of Thermal Properties of Biomaterials," Annual Review of Biophysics and Bioengineering, vol. 4, (1), pp. 43-80, 1975.

[8] Lide and David R., ed. 2009. *CRC Handbook of Chemistry and Physics*, Boca Raton, Florida: CRC Press.

[9] K. Yazawa and D. Kendig. "Understanding the Thermoreflectance Coefficient for High Resolution Thermal Imaging of Microelectronic Devices" Electronics Cooling. Number 1, Thermal Imaging, Volume 19.

[10] I. Cohen, B. Lustman and J. D. Eichenberg, 1961, "Measurement of the thermal conductivity of metal clad uranium oxide rods during irradiation," Journal of Nuclear Materials, vol. 3, (3), pp. 331-353.

[11] A. Ångström and T. Matsumura, 2008, "Post irradiation Examinations focused on Fuel Integrity of spent BWR-MOX and PWR-UO_2 Fuels Stored for 2-0 Year," Nucl. Eng. Des., 238(5), pp. 1250-1259.

[12] Y. Takahashi and M. Murabayashi, 1975, “Measurement of Thermal Properties of Nuclear Materials by Laser Flash Method,” J. Nucl. Sci. Technol., 12(3), pp. 133-144.

[13] Y. Zhao, “Pulsed Photothermal Reflectance Measurement of the Thermal Conductivity of Sputtered Nitride Thin Films,” Journal of Applied Physics.

[14] Z. Hua, 2013, “Hybrid Photothermal Technique for Microscale Thermal Conductivity Measurement,”.

[15] A. Rosencwaig and A. Gersho, 1976, “Theory of the Photoacoustic Effect with Solids,” J. Appl. Phys., 47(1), pp. 64-69.

[16] A.C. Tam, 1989, “Photothermal Techniques in Material Characterization Applications，” Review of Progress in Quantitative Nondestructive Evaluation. Springer, Boston, MA.

[17] M. Olmstead, N. Amer, D. Kohn, Fournier and A. Boccara, 1983, “Photothermal Displacement Spectroscopy: An Optical Probe for Solids and Surfaces,” Appl. Phys. A Mater. Sci. Process., 32(3), pp. 141-154.

[18] G. Benedetto, R. Spagnolo and L. Boarino, 1993, “Photothermal Displacement Technique: A Method to Determine the Variation of Thermal Conductivity versus Temperature in Silicon,” Rev. Sci. Instrum., 64(8), pp. 2229-2232.

[19] D.K. Yao, C. Zhang, K. Maslov and L. Wang, 2014, “Photoacoustic Measurement of the Gruneisen Parameter of Tissue,” Journal of biomedical optics. 19. 17007. 10.1117/1.JBO.19.1.017007.

[20] W. Parker, R. Jenkins, C. Butler, and G. Abbott, 1961, "Flash Method of Determining Thermal Diffusivity, Heat Capacity, and Thermal Conductivity," J. Appl. Phys., 32(9), pp.1679-1684.

[21] S. Corbin, 2012, “Thermal Diffusivity by the Laser Flash Technique,” Thermal Analysis.

[22] H. Weakliem and H. Gronbeck, 1979, “Temperature Dependence of the Optical Properties of Silicon,” J.Appl. Physi. 50(3), pp. 5266-5269.

[23] S. Min, J. Blumm, and A. Lndemann, 2007, “A New Laser Flash System for Measurement of the Thermophysical Properties,” Thermochim. Acta, 455 (1), pp.46-49.

[24] W. Nunes dos Santos, P. Mummery and A. Wallwork, 2005, “Thermal Diffusivity of Polymers by the Laser Flash Technique,” Polym. Test., 24(5), pp. 628-634.

[25] S. Min, J. Blumm and A. Lindemann, 2007, “A New Laser Flash System for Measurement of the Thermophysical Properties,” Thermochim. Acta, 455(1), pp. 46-49.

[26] V. Casalegno, P. Vavassori, M. Valle, M. Ferraris, M. Salvo and G. Pintsuk, 2010, “Measurement of Thermal Properties of a Ceramic/Metal Joint by Laser Flash Method,” J. Nucl. Mater., 407(2), pp. 83-87.

[27] P. Nordal, O.K. Svein, 1977, “Photoacoustic spectroscopy on ammonium sulphate and glucose powders and their aqueous solutions using a Co2 laser,” Optics Communications, Vol: 22, Issue 2, Page: 185-189

[28] P. Nordal and S. Kanstad, 1979, “Photothermal Radiometry,” Phys. Scripta, 20(5-6), p. 659.

[29] R. Santos, and L. Miranda, 1981, “Theory of the Photothermal Radiometry with Solids,”J. Appl. Phys., 52(6), pp. 4194-4198

[30] K. Horne, H. Ban, A. Mandelis and A. Matvienko, 2012, "Photothermal Radiometry Measurement of Thermophysical Property Change of an Ion-irradiated Sample," Mater. Sci. Eng., B, 177(2), pp. 164-167.

[31] R. D. Tom, E.P. Ohara and D. Benin, 1982, “A Generalized Model of Photothermal Radiometry,” J. Appl. Phys., 53(8), pp. 5392-5400.

[32] J. Martan, O. Herve and V. Lang, 2007, “Two-detector Measurement System of Pulse Photothermal Radiometry for the Investigation of the Thermal Properties of Thin Films,” J. Appl. Phys., 102(6), p. 064903.

[33] J. Caberero and F. Audubert, 2009, “Thermal conductivity of SiC after Heavy Ions Irradiation,” Journal of Nuclear Materials, 01/2010, Volume 396, Issue 2-3.

[34] H. Weakliem and D. Redfield, 1979, "Temperature Dependence of the Optical Properties of Silicon," J. Appl. Phys., 50(3), pp. 1491-1493.

[35] Rosencwaig, A., Opsal, J., Smith, and Willenborg, D., 1985, "Detection of Thermal Waves Through Optical Reflectance," Appl. Phys. Lett., 46(11), pp. 1013-1015.

[36] M. Reichling, and H. Gronbeck, 1994, "Harmonic Heat Flow in Isotropic Layered Systems and Its Use for Thin Film Thermal Conductivity Measurements," J. Appl. Phys., 75(4), pp. 1914-1922.

[37] A. Maznev, Hartmann and M. Reichling, 1995, "Thermal Wave Propagation in Thin Films on Substrates," J. Appl. Phys., 78(9), pp. 5266-5269.

[38] T. Yagi, N. Taketoshi and H. Kato, 2004, "Distribution Analysis of Thermal Effusivity for Sub-micrometer YBCO Thin Films Using Thermal Microscope," Physica C: Superconductivity, 412, pp. 1337-1342.

[39] C. Paddock and G. L. Eesley, 1986, "Transient Thermoreflectance from Thin Metal Films," J. Appl. Phys., 60(1), pp. 285-290.

[40] A. Salazar, A. Sanchez-Lavega and J. Terron, 1998, "Effective Thermal Diffusivity of Layered Materials Measured by Modulated Photothermal Techniques," J. Appl. Phys., 84(6), pp. 3031-3041.

[41] B. Li, J. Roger, L. Pottier and D. Fournier, 1999, "Complete Thermal Characterization of Film-on-substrate System by Modulated Thermoreflectance Microscopy and Multiparameter Fitting," J. Appl. Phys., 86(9), pp. 5314-5316.

[42] A. Mansanares, T. Velinov, Z. Bozoki, D. Fournier and A. Boccara, 1994, "Photothermal Microscopy: Thermal Contrast at Grain Interface in Sintered Metallic Materials," J. Appl. Phys., 75(7), pp. 3344-3350.

[43] Z. Hua and H. Ban ,2012, “Spatially Localized Measurement of Thermal Conductivity Using a Hybrid photothermal technique,” Journal of Applied Physics, 05/2012, Volume 111, Issue 10.

[44] A. Maznev, J. Hartmann and M. Reichling, 1995, "Thermal Wave Propagation in Thin Films on Substrates," J. Appl. Phys., 78(9), pp. 5266-5269.

[45] Z.Hua, H. Ban, M. Khafizov, R. Schley, R. Kennedy and D.H. Hurley, 2012, "Spatially Localized Measurement of Thermal Conductivity Using a Hybrid Photothermal Technique," J. Appl. Phys., 111(10), p. 103505.

[46] Z.Hua, and H. Ban, 2017, “Thermal Diffusivity Measurement of Focused-Ion-Beam Fabricated Sample using Photothermal Reflectance Technique,” Review of Scientific Instruments. 88(5): p. 054901.